

# CMIP6 models underestimate the Holton-Tan effect

Dillon Elsbury<sup>1</sup>, Yannick Peings<sup>1</sup>, and Gudrun Magnusdottir<sup>1</sup>

<sup>1</sup>Department of Earth System Science

November 22, 2022

## Abstract

The teleconnection between the Quasi-Biennial Oscillation (QBO) and the Arctic polar vortex is investigated using Coupled Model Intercomparison Project phase 6 (CMIP6) models. We use 14 CMIP6 models, reanalysis, three experiments with prescribed QBOs, one of which has no free polar stratospheric variability, and branched runs in which a QBO is imposed in runs previously devoid of a QBO. Each CMIP6 model underestimates the Holton-Tan effect (HTE), the weakening of the polar vortex with QBO easterlies in the lower stratosphere. To establish why, 850 Kelvin potential vorticity (PV) maps are used to study zonal asymmetries in the teleconnection. The QBO initiates the HTE by promoting equatorward (poleward) intrusion of high (low) PV over mid-latitude Asia (60°E-120°E). The presence of the PV intrusion in a model response is highly correlated with polar cap warming and the HTE. Models with stronger 10 hPa QBO amplitudes generally include the PV intrusion.

## Hosted file

gr1\_cmip6\_models\_underestimate\_the\_hte\_supplementary.docx available at <https://authorea.com/users/311288/articles/599642-cmip6-models-underestimate-the-holton-tan-effect>

1

2

## CMIP6 models underestimate the Holton-Tan effect

3

4 **Dillon Elsbury<sup>1</sup>, Yannick Peings<sup>1</sup>, and Gudrun Magnusdottir<sup>1</sup>**

5 <sup>1</sup>University of California, Irvine, Department of Earth System Science

6 Corresponding author: Dillon Elsbury ([delsbury@uci.edu](mailto:delsbury@uci.edu)): orcid: 0000-0002-3730-9226

### 7 **Key Points:**

8 • The CMIP6 models underestimate the weakening of the polar vortex expected  
9 when QBO easterlies exist in the tropical lower stratosphere

10 • Potential vorticity (PV) maps reveal that pooling of PV over mid-latitude Asia is  
11 important for coupling the QBO with the polar vortex

12 • The models underestimate the teleconnection because the 10 hPa QBO  
13 westerlies are too weak and too narrow

14 **Abstract**

15 The teleconnection between the Quasi-Biennial Oscillation (QBO) and the Arctic polar  
16 vortex is investigated using Coupled Model Intercomparison Project phase 6 (CMIP6)  
17 models. We use 14 CMIP6 models, reanalysis, three experiments with prescribed  
18 QBOs, one of which has no free polar stratospheric variability, and branched runs in  
19 which a QBO is imposed in runs previously devoid of a QBO. Each CMIP6 model  
20 underestimates the Holton-Tan effect (HTE), the weakening of the polar vortex with  
21 QBO easterlies in the lower stratosphere. To establish why, 850 Kelvin potential vorticity  
22 (PV) maps are used to study zonal asymmetries in the teleconnection. The QBO  
23 initiates the HTE by promoting equatorward (poleward) intrusion of high (low) PV over  
24 mid-latitude Asia (60°E-120°E). The presence of the PV intrusion in a model response is  
25 highly correlated with polar cap warming and the HTE. Models with stronger 10 hPa  
26 QBO amplitudes generally include the PV intrusion.

27

28 **Plain Language Summary**

29 In the tropics at altitudes between two and three times as high as commercial airplanes  
30 cruise, the winds alternate between blowing to the east for about a year before  
31 switching direction and blowing to the west for the next year. This pattern of winds is  
32 called the Quasi-Biennial Oscillation (QBO). Despite being high up in the tropical  
33 atmosphere, the QBO affects the global circulation in ways that ultimately influence  
34 regional weather. One example of this occurs during winter, when the QBO changes the  
35 strength of the jet-stream. Although scientists have known about this phenomenon for

36 over 40 years, this long-distance relationship is complicated. Models of the coupled  
37 land, ocean, atmosphere system have steadily improved at representing the QBO.  
38 These models also represent the QBO's relationship with the jet-stream, but each  
39 model does it differently. We evaluate how the models perform in this study. The  
40 difference between models that represent the QBO-jet-stream relationship well and  
41 models that do not teaches us more about the relationship. We learn here that the QBO  
42 begins communicating with the jet by changing the atmospheric circulation 30  
43 kilometers above Asia, nearly over the Tibetan Plateau. This phenomenon is best  
44 represented by models that have stronger QBOs.

45

## 46 **1 Introduction**

47 The Quasi-Biennial Oscillation (QBO) influences the global circulation through a suite of  
48 teleconnections (Gray et al. 2018). It modulates tropical convection (Son et al. 2017),  
49 upper tropospheric mid-latitude flow (Wang et al. 2018; Hitchman et al. 2021), and polar  
50 stratospheric flow in the southern (Yamashita et al. 2018) and northern hemispheres  
51 (Holton and Tan 1980; Lu et al. 2020). Each teleconnection is sensitive to the QBO's  
52 structure, its meridional extent (Hansen et al. 2013), the configuration of its easterly and  
53 westerly jets (Garfinkel et al. 2012; Gray et al. 2018), its vertical extent (Andrews et al.  
54 2019), and how deep it reaches into the lower stratosphere (Collimore et al. 2003). Now  
55 with the Coupled Model Intercomparison Project 6 (CMIP6) models spontaneously  
56 generating the QBO, there is variability in how the models represent its structure  
57 (Richter et al. 2020). This suggests that there is variability in how the models represent  
58 the QBO teleconnections (Rao et al. 2020a,b). This study focuses on one of these

59 teleconnections, the boreal winter polar stratospheric response to the QBO, the Holton-  
60 Tan effect (HTE, Holton and Tan 1980). We have two goals: (1) better understand why  
61 the CMIP6 models underestimate the HTE (Fig. 1) while (2) also learning how the  
62 middle stratospheric, 850 Kelvin, branch of the teleconnection varies over longitude.

63

64 When QBO westerlies are in the middle stratosphere (10 hPa) and QBO easterlies in  
65 the lower stratosphere (50 hPa), the polar vortex is weaker than in climatology. This  
66 configuration of the QBO, denoted QBO<sub>E50</sub>, influences where planetary wave breaking  
67 occurs in the stratosphere (Hitchman and Husesmann 2009; Lu et al. 2020). QBO  
68 easterlies concentrate planetary waves and their breaking into the northern hemisphere  
69 (Holton and Tan 1980; Lu et al. 2020). The QBO induced mean meridional circulation  
70 (QBO-MMC) is also important for this teleconnection.

71

72 The QBO-MMC acts as a residual mean meridional circulation that maintains the  
73 dynamically forced temperature response to the QBO against radiative relaxation  
74 (Plumb and Bell 1982; Pahlavan et al. 2021; Hitchman et al. 2021). Westerly (easterly)  
75 QBO shear coincides with tropical warming (cooling), which is generated by adiabatic  
76 descent (ascent). At subtropical to mid-latitudes, the QBO-MMC induces vertical motion  
77 in the opposite direction of that in the tropics, yielding opposite temperature responses  
78 (Fig. 1q). The QBO-MMC changes the mid-latitude middle stratospheric mean flow  
79 geometry, forcing more poleward refraction of planetary waves (Garfinkel et al. 2012; Lu  
80 et al. 2014), which would otherwise propagate equatorward. This weakens the polar  
81 vortex.

82

83 It is not clear how this process varies over longitude. We hypothesize that it does as the  
84 QBO demonstrates zonally asymmetric teleconnections elsewhere. It has unique  
85 impacts on the North Pacific and North Atlantic jets (Wang et al. 2018). Further, we find  
86 that the QBO preferentially communicates with the mid-latitude North Pacific lower  
87 stratosphere by inducing more planetary wave absorption there relative to other  
88 longitudes (Elsbury et al. 2021). A more speculative hypothesis is that the QBO's  
89 zonally asymmetric structure (Hamilton et al. 2004; Hitchman and Huesmann 2009;  
90 Tegtmeier et al. 2020) predisposes it to have zonally asymmetric impacts on the  
91 extratropical circulation.

92

## 93 **2 Methods**

94 The HTE is analyzed over the 1850-2014 period using the same historical CMIP6  
95 models used by Richter et al. (2020) to facilitate comparison between the extratropical  
96 responses (this study) and the QBO qualities in each model (their study). The CMIP6  
97 responses to the QBO are compared to 1979-2019 ERA5 reanalysis (Hersbach et al.  
98 2020).

99

100 Four experiments with the specified chemistry version of the Whole Atmosphere  
101 Community Climate Model (SC-WACCM4, Smith et al. 2014) use a prescribed QBO  
102 and are therefore useful for comparing with the CMIP6 models. The model domain is  
103 the surface up to 145 kilometers over 66 vertical levels with horizontal resolution of 1.9°  
104 latitude, 2.5° longitude. To simulate the QBO, the tropical stratospheric winds from 86

105 hPa-4 hPa and 22°S-22°N are relaxed toward a climatological 28-month QBO cycle  
106 derived from radiosondes (Hansen et al. 2013). The first of the experiments, referred to  
107 as PAMIP-WCSC, is a 1500-year simulation with a repeating annual cycle of sea  
108 surface temperature (SST) corresponding to present-day climate and a suite of different  
109 Arctic sea ice forcings (we neglect a potential influence of Arctic sea ice conditions on  
110 the QBO teleconnections). The second experiment, AMIP-WCSC, is a 370-year dataset  
111 made up of 10 ensemble members, run from 1978 to 2016, forced by the observed  
112 chronology of SST and sea ice variability. The third experiment, CPS-WCSC, is a 300-  
113 year simulation forced in the same way as PAMIP-WCSC except the polar stratospheric  
114 variability poleward of 60°N is relaxed toward a climatological polar stratospheric state  
115 allowing us to diagnose the influence of the QBO on the atmosphere in the absence of a  
116 polar stratospheric response to the QBO. The fourth experiment allows us to diagnose  
117 the transient atmospheric response to imposing the QBO. A 100-year control simulation  
118 devoid of the prescribed QBO is run and restarts are saved for each November 1<sup>st</sup>. We  
119 branch from November 1<sup>st</sup> and then impose the QBO<sub>E50</sub> profile. The QBO propagates  
120 downward and the runs last until January 31<sup>st</sup>. More details on PAMIP-WCSC, CPS-  
121 WCSC, and the transient runs are given in Elsbury et al. (2021).

122

123 Throughout the manuscript, anomalies are calculated as deviations from the seasonal  
124 cycle. These anomalies are then subsampled by QBO phase. The QBO<sub>E50</sub> index can be  
125 defined using westerlies at 10 hPa or easterlies at 50 hPa. Both yield similar results.  
126 However, the latter captures non-QBO variability for some models. Therefore, the  
127 QBO<sub>E50</sub> index is defined as the December-January (DJ) time averaged, longitudinally

128 averaged, and latitudinally averaged winds between 5°S and 5°N at 10 hPa that exceed  
129 2.5 m/s. Further, similar results are obtained using the phase angle 30 hPa QBO index  
130 of Huang et al. (2012). This index allows for more control in picking the vertical structure  
131 of the QBO we are interested in, e.g., easterlies at 50 hPa (Fig. S1). Results are  
132 consistent for all three QBO indices. Here we present results using the QBO<sub>E50</sub> index  
133 and have phase angle duplicates of Fig. 1 and 4 in supplementary (Fig.S2, Fig. S3).

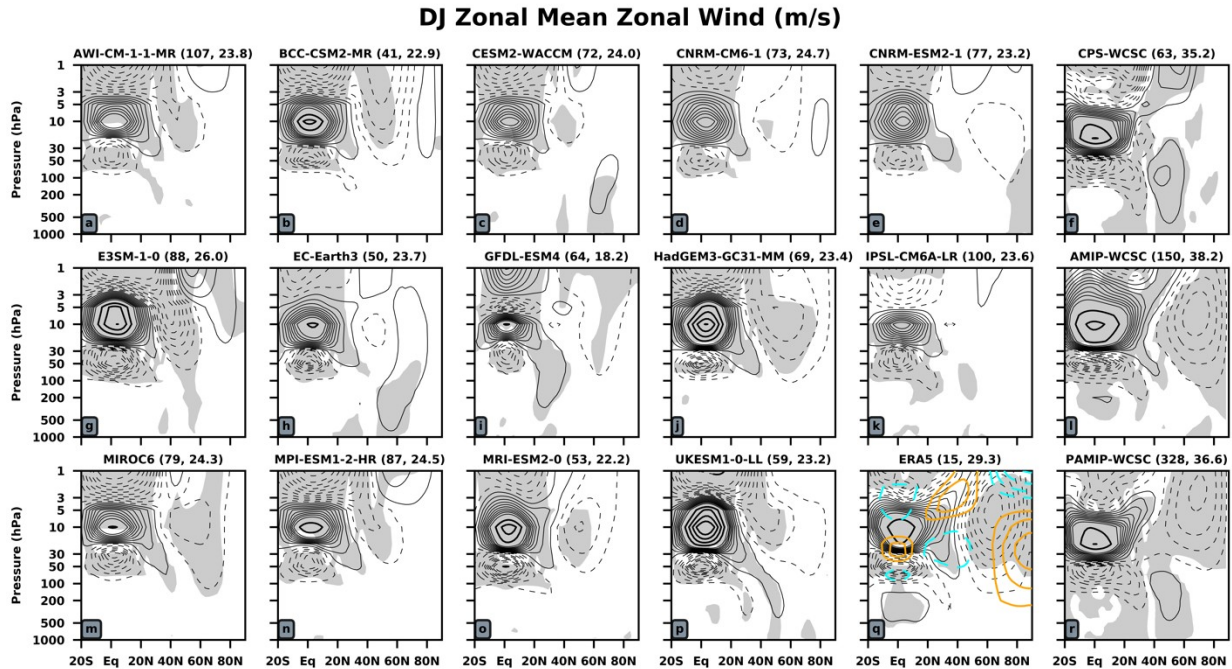
134

### 135 **3 Results**

#### 136 **3.1 Zonal mean zonal wind**

137 Figure 1 shows zonal mean zonal wind anomalies for all 18 datasets. The models both  
138 overestimate (1b, g, j, o, p) and underestimate (all others) the peak 10 hPa QBO  
139 westerlies relative to ERA5 (shown by Richter et al. 2020). The QBO westerlies extend  
140 upward and poleward between 20°N-40°N in ERA5, but they are confined equatorward  
141 in CMIP6 models. Each CMIP6 QBO is narrow relative to ERA5 (10 hPa QBO widths  
142 printed above plots).

143



144

145 Figure 1: DJ zonal mean zonal wind anomalies. Thin contours show anomalies between  $\pm 8.5$  m/s with intervals of  $\pm 1$  m/s. Thick  
 146 contours correspond to  $\pm 10, 15, 20 \dots$  m/s. Gray shading denotes statistical significance,  $p$ -values  $< 0.05$  via a student's  $t$ -test, when  
 147 comparing QBO<sub>E50</sub> anomalies to all other anomalies. To the right of model titles is the number of DJ periods averaged together to  
 148 make each composite and the 10 hPa latitudinal width of the QBO. Widths are calculated by applying the "half-maximum" method of  
 149 Richter et al. (2020) and Bushell et al. (2020) to the anomalous 10 hPa response from each plot. Warm (cool) temperature  
 150 anomalies are shown on Fig. 1q with  $\pm 1$  K contours.

151

152 The 50 hPa peak QBO easterlies match ERA5 in four cases (1g, j, o, p) and are  
 153 underestimated otherwise. Each unique QBO coincides with unique tropical  
 154 stratospheric temperature perturbations (not shown), which the QBO-MMC must  
 155 maintain against radiative relaxation. Therefore, the QBO-MMC differs in each model.  
 156 Prescribing the QBO ensures that it has sufficient lower stratospheric amplitude. The  
 157 QBO, in the absence of a HTE, pushes the tropospheric jet poleward (CPS, Fig. 1f).  
 158 This is moderated by an equatorward jet shift in AMIP and PAMIP (Fig. 1l,r) due to a  
 159 warm polar stratosphere caused by the HTE (Elsbury et al. 2021, Fig. 6). These

160 experiments with prescribed QBOs show that when a realistic QBO exists in the model,  
161 teleconnections more closely resemble observations, notably the HTE.

162

163 While some models simulate a weakening of the polar stratospheric winds (BCC-CSM2-  
164 MR, HadGEM3-GC31-MM, MIROC6, UKESM1-0-LL), each model underestimates the  
165 HTE relative to ERA5 (Fig. 1q) and the prescribed QBO runs (Fig 1l, r). AWI-CM-1-1-  
166 MR, E3SM-1-0, MPI-ESM1-2-HR, and MRI-ESM2-0 each have extratropical easterly  
167 anomalies, but they are not at polar latitudes. Underestimation of the HTE occurs with  
168 all three QBO indices (Fig. S2). This should hinder stratospheric interaction with the  
169 tropospheric jet.

170

### 171 **3.2 Zonally asymmetric middle stratospheric teleconnection**

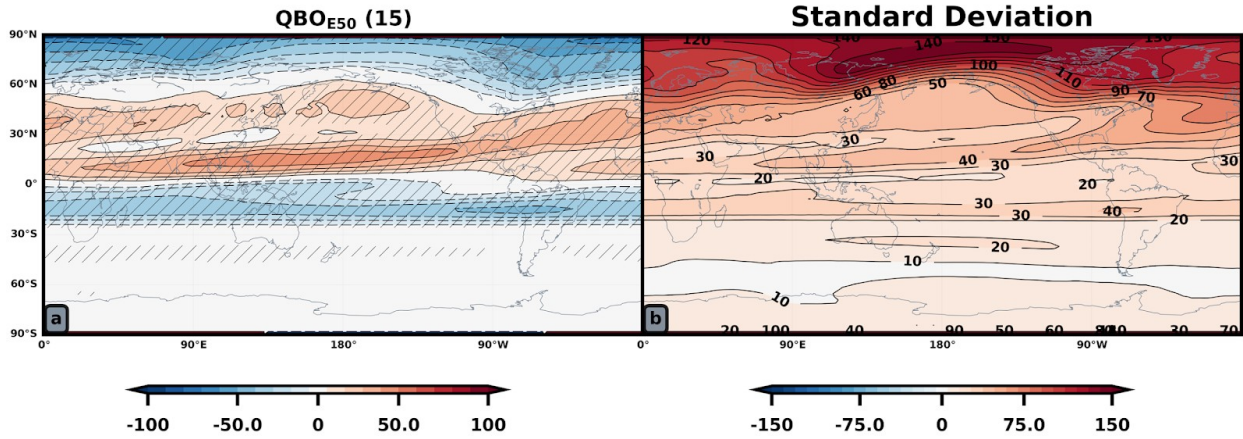
172 Before assessing the representation of the middle stratospheric HTE, we need to  
173 establish what this teleconnection looks like in a zonally asymmetric sense. Figure 2  
174 shows potential vorticity (PV) on the 850 Kelvin isentropic surface (approximately  
175 10hPa) associated with  $QBO_{E50}$  in ERA5. The standard deviation of the field shows that  
176 PV varies between 20 and 50 PVU from 30°N to 30°S with larger variability in the North  
177 Atlantic mid-latitudes than in the North Pacific (Fig. 2b). The largest variations occur at  
178 polar latitudes, especially over the North Pacific.

179

180 Relative to the standard deviation, the  $QBO_{E50}$  dominates the tropical and subtropical  
181 850 K PV variability (Fig. 2a). At polar latitudes, the polar vortex is most disturbed over  
182 the North Atlantic where low PV anomalies peak at -60 PVU, about 50% of the |

183 standard deviation| there. Fig. 2a mirrors the DJ 850 K first empirical orthogonal  
 184 function, which accounts for 36% of the variance (Fig. S4).  
 185

## ERA5 DJ 850 K PV (PVU)



186

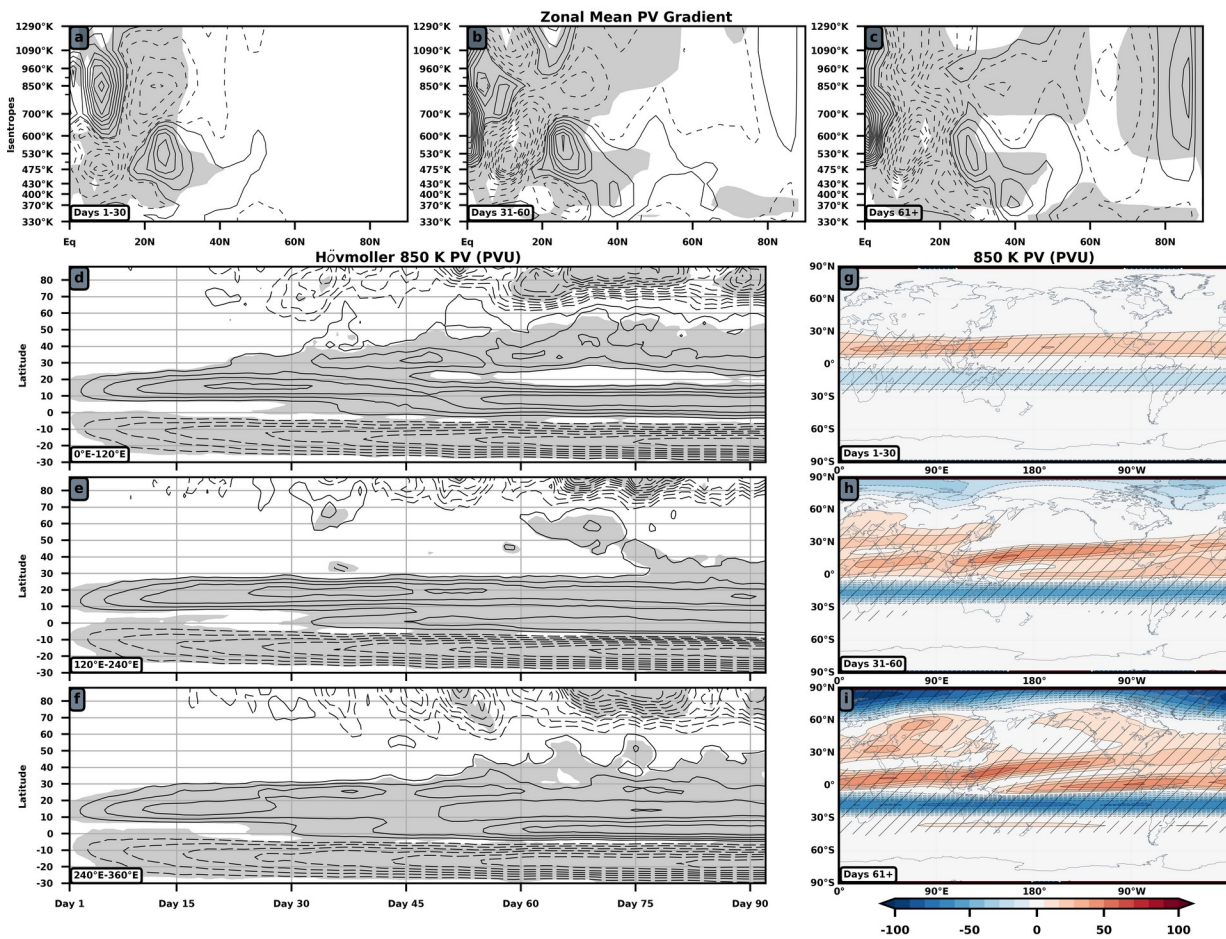
187 Figure 2: ERA5 DJ 850 Kelvin PV anomalies. Anomalies are deviations from the seasonal cycle for QBO<sub>E50</sub> indices. Hatching  
 188 denotes statistical significance, p-values < 0.05 via a student' t-test, when comparing QBO<sub>E50</sub> anomalies to all other anomalies. The  
 189 contour interval in line and shading for all panels is +/- 10 PVU. Fifteen DJ seasons are used to make the composite (a). Panel (b)  
 190 shows the standard deviation of the field with contour intervals 10, 20, 30... PVU.  
 191

192 Two bands of anomalous PV span the tropics, negative in the southern hemisphere,  
 193 positive in the northern hemisphere (Fig. 2a). This is the signature of the QBO-MMC.  
 194 Shown by Hitchman and Huesmann (2009), the QBO-MMC converges toward the base  
 195 of the QBO westerlies, “pinching” together the PV contours: high PV from the northern  
 196 hemisphere and low PV from the southern hemisphere are concentrated nearer the  
 197 tropics. The negative PV anomaly in the southern hemisphere shows some zonal  
 198 asymmetry while the northern hemisphere positive PV band shows strong variation over  
 199 longitude.

200

201 Since internal variability may convolute these PV results, we look for these signatures in  
 202 dedicated perturbation experiments. Figure 3 shows the evolution of the PV field once a  
 203 downward propagating QBO<sub>E50</sub> profile is imposed in the control simulation devoid of a  
 204 QBO. Anomalies are calculated as the difference between the transient runs and control  
 205 runs from which the transient simulations are branched.  
 206

### QBO<sub>E50</sub> Transient PV Anomalies



207  
 208 Figure 3: Anomalies after imposing a QBO<sub>E50</sub> profile in the transient runs. (a-c): Zonal mean meridional PV gradient for successive  
 209 30-day periods after branching: dashed-negative (solid-positive) contours begin at negative (positive)  $1 \times 10^{-7} \text{ K} \cdot \text{m} \cdot \text{kg}^{-1} \cdot \text{s}^{-1}$  and  
 210 decrease (increase) by negative (positive)  $5 \times 10^{-7} \text{ K} \cdot \text{m} \cdot \text{kg}^{-1} \cdot \text{s}^{-1}$  intervals. The responses at each isentrope are multiplied by  $(\theta/350)^{1/2}$   
 211 <sup>1/2</sup> to account for logarithmic change in PV with height. (d-f): Latitude-time Hövmollers of 850 Kelvin PV ( $\pm 10$  PVU) averaged over  
 212  $0^\circ\text{E}-120^\circ\text{E}$  (d),  $120^\circ\text{E}-240^\circ\text{E}$  (e), and (f)  $240^\circ\text{E}-360^\circ\text{E}$ . Gray shading denotes statistical significance in (a-f), p-values  $< 0.05$  via a

213 student's t-test, when comparing QBO<sub>E50</sub> and control responses. (g-h) Maps of 850 K PV (+/- 10 PVU) anomalies with hatching  
214 denoting statistical significance.

215

216 Figs. 3a-c shows change in the meridional gradient of the zonal mean PV,  $P_{\varphi}$ , once the  
217 QBO<sub>E50</sub> is imposed. Negative anomalies mean that the PV gradient is decreased and  
218 linear wave propagation into the region is less likely while the opposite holds true for  
219 regions with positive anomalies. During days 1-30, QBOW is located around 850 K and  
220 QBOE around 530 K. Planetary waves may propagate through the 850 K westerlies, but  
221 not the 530 K easterlies (Fig. 3a).  $P_{\varphi}$  weakens in the middle stratosphere between 30°N-  
222 50°N during days 31-60 indicating reduced likelihood for equatorward propagation (Fig.  
223 3b). Beyond day 61, the polar stratospheric gradient weakens and this signal  
224 propagates downward (Fig. 3c). How does the spatiotemporal evolution of PV look on a  
225 horizontal surface, if we do not take a zonal average?

226

227 During the first 30 days at 850 K, the QBO-MMC spins up (Figs. 3g-i). The two  
228 anomalous PV bands indicate equatorward motion of the QBO-MMC from both  
229 hemispheres and the signal is almost zonally symmetric with more pooling of high PV  
230 near Asia (Fig. 3g). During the next 30 days, the positive PV anomalies become more  
231 zonally asymmetric, tilting out of the tropics toward the east (Fig. 3h). The evolution of  
232 the anomalous negative PV gradient poleward seen in the zonal mean occurs over  
233 Eurasia between 30°N and 50°N (Fig. 3h). Pooling of high PV over these continents is  
234 consistent with dilution of high PV over the pole during the last 32 days of the  
235 simulations (Fig. 3i).

236

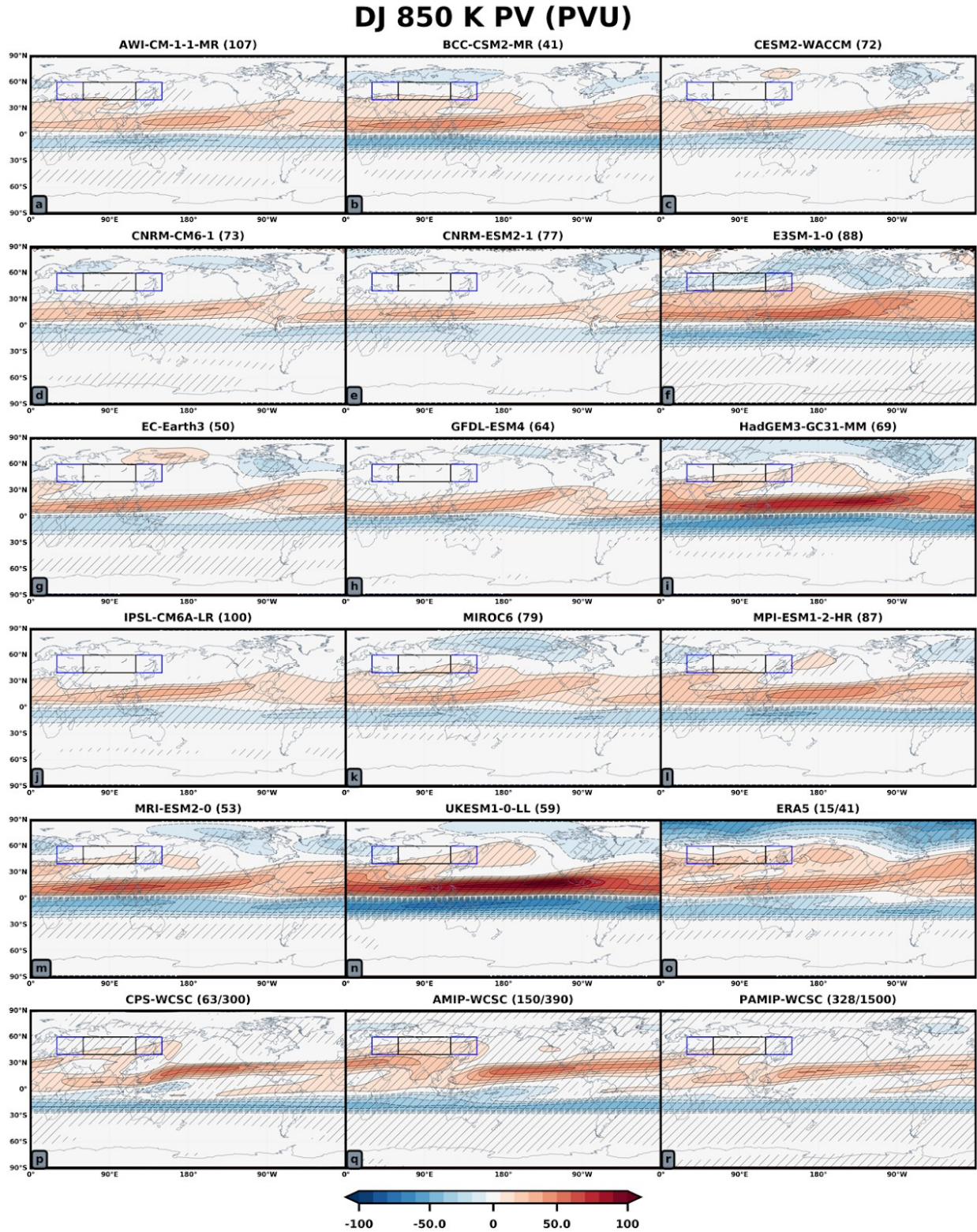
237 Latitude-time Hövmollers make clear the importance of the Eurasia sector for coupling  
238 the QBO with the polar vortex (Figs. 3d-f). Equatorward (poleward) intrusion of high  
239 (low) PV occurs between 0°E-120°E during days 30-45 (Fig. 3d). Importantly, this  
240 anomalous flattening of the PV gradient (Fig. 3d) leads the other sectors (Fig. 3e-f). Fig.  
241 3 suggests that the HTE begins in the middle stratosphere (Fig. 3a-c), particularly over  
242 Eurasia (Fig. 3d,h).

243

244 While the PV intrusion is broadly located over Africa, Europe, and Asia, subsequent  
245 results will show that the PV response over mid-latitude Asia is most important for the  
246 HTE. Therefore, we hereafter refer to this regional PV response as the “PV intrusion” or  
247 “Asia  $P_{\psi}$ .”

248

### 249 **3.3 Middle stratosphere in the CMIP6 models**



250

251 Figure 4: DJ 850 K PV anomalies for the 18 datasets. Contour intervals are +/- 10 m/s. Hatching denotes statistical significance, p-  
 252 values < 0.05 via a student's t-test, when comparing  $QBO_{E50}$  anomalies to all other anomalies. Black and blue rectangles denote  
 253 where the anomalous  $p$  is highly correlated with polar cap warming (Table S1).

254

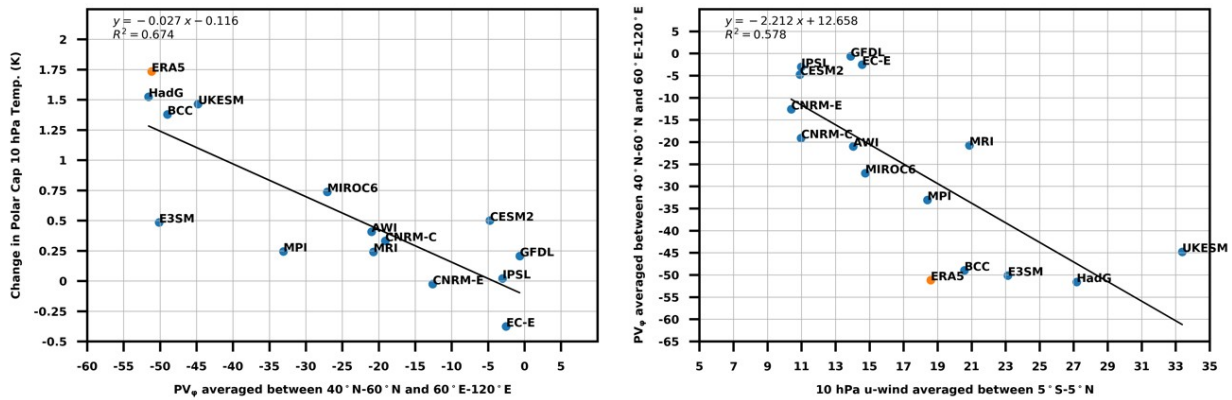
255 Figure 4 shows 850 K PV anomalies for each model. From Fig. 1, the models that  
256 exhibit extratropical easterlies at polar latitudes (BCC-CSM2-MR, HadGEM3-GC31-MM,  
257 MIROC6, UKESM1-0-LL) or mid-latitudes (AWI-CM-1-1-MR, E3SM-1-0, MPI-ESM1-2-  
258 HR, MRI-ESM2-0) exhibit intrusion of high PV over mid-latitude Asia. Models with  
259 weaker HTEs (CESM2-WACCM, CNRM-CM6-1, CNRM-ESM2-1, EC-Earth3, GFDL-  
260 ESM4, IPSL-CM6A-LR) exhibit no pooling of PV over Asia. The CMIP6 PV intrusions  
261 are equatorward of the intrusions in ERA5 or SC-WACCM4, suggesting why the CMIP6  
262 extratropical easterly anomalies are ubiquitously equatorward of the polar stratosphere  
263 in Fig. 1. Note that every dataset's QBO is zonally asymmetric with stronger flow around  
264 Indonesia or the Indian Ocean, which may explain the location of the PV intrusion (Fig.  
265 S5).

266

267 Enhanced PV over Asia indicates anomalous cyclonic flow there. Stronger westerlies on  
268 its equatorward flank should strengthen  $P_{\varphi}$  and reduce wave breaking. Stronger  
269 easterlies on its poleward flank should weaken  $P_{\varphi}$  and reduce wave propagation.  
270 Indeed, studies using reanalysis (Fig. 3b of Lu et al. 2014) and model experiments  
271 (Garfinkel et al. 2012) show that  $QBO_{E50}$  suppresses climatological equatorward  
272 planetary wave propagation at 850 K between 30°N and 50°N in favor of anomalous  
273 poleward propagation. These PV results corroborate those studies and we add and  
274 emphasize that this process occurs over Asia.

275

276 Fig. 5 suggests that the PV intrusion is associated with the HTE. It establishes the  
 277 relation between the anomalous polar cap temperatures at 10 hPa and  $P_\varphi$  averaged  
 278 between 40°N and 60°N over various 60° longitude windows (Table S1). Various 60°  
 279 longitude windows are used to see over what longitudes  $P_\varphi$  is most strongly associated  
 280 with the polar cap temperature anomalies. Correlations exceed 0.7 from 30°E-150°E  
 281 and peak at 0.82 from 60°E-120°E (Table S1). This is where the PV intrusion is located  
 282 (enclosed by rectangles in Fig. 4). Fig. 5a depicts the relationship between Asia  $P_\varphi$  and  
 283 polar cap temperatures. The more negative Asia  $P_\varphi$  is, the warmer the polar cap is (Fig.  
 284 5a).



285  
 286 Figure 5: Left: The anomalous meridional PV gradient ( $P_\varphi$ ) over Asia is compared to the anomalous 10 hPa polar cap (60°N+)  
 287 temperature.  $P_\varphi$  is not divided by the radius of Earth when calculating it. Right: The anomalous 10 hPa QBO, longitudinally averaged  
 288 and cosine weighted latitudinally averaged zonal winds between 5°S-5°N, of Figure 1 are compared to  $P_\varphi$  over Asia.

289  
 290 Asia  $P_\varphi$  is a direct response to the QBO – it does not result from the HTE. Indeed, the  
 291 PV intrusion exists in the CPS 850 K response, which reveals the impact of the QBO in  
 292 the absence of a polar stratospheric response (Fig. 4r). Furthermore, imposing the QBO  
 293 in the transient simulations promoted the PV intrusion (Fig. 3). Regression between the  
 294 10 hPa QBO westerly velocity and Asia  $P_\varphi$  shows that stronger QBO winds equate to

295 more negative Asia  $P_\varphi$  (Fig. 5b). Citing the strong relationship between Asia  $P_\varphi$  and  
296 polar cap temperatures, underestimation of the 10 hPa QBO amplitudes is *partly*  
297 suppressing the HTE.

298

## 299 **4 Discussion**

### 300 **4.1 Importance of the QBO-MMC**

301 Stronger QBOs have larger effects on the extratropical circulation. Of the 14 CMIP6  
302 models, the eight with strongest 10 hPa QBO westerlies are BCC-CSM2-MR,  
303 HadGEM3-GC31-MM, MIROC6, UKESM1-0-LL, AWI-CM-1-1-MR, E3SM-1-0, MPI-  
304 ESM1-2-HR, and MRI-ESM2-0 (Fig. 5b, compare with Fig. 2b of Richter et al. 2020).

305 The first four models feature some weakening of the polar vortex while the latter four  
306 exhibit anomalous easterlies equatorward of the polar vortex. The models with the  
307 weakest 10 hPa QBO westerlies exhibit much weaker easterlies everywhere in the  
308 stratosphere (Fig. 1c, d, e, h, i, k).

309

310 Our Figs. 4 and 5b show that models with stronger 10 hPa QBO amplitudes feature  
311 stronger PV intrusions over Asia. Garfinkel and Hartmann (2011, Fig. 6) show that  
312 stronger QBOs have stronger QBO-MMCs, which have larger effects on the  
313 extratropical circulation. A speculation then is that the PV intrusion may be the  
314 extratropical signature of the QBO-MMC. By underestimating this feature, which  
315 confines planetary waves to higher latitudes (Lu et al. 2014), the models underestimate  
316 the HTE.

317

## 318 **4.2 Limitations of our argument**

319 Underestimating the 10 hPa QBO amplitudes is not the only factor hindering the HTEs.  
320 For instance, HadGEM3-GC31-MM and UKESM1-0-LL both overestimate the 10 hPa  
321 QBO winds and still underestimate the weakening of the polar vortex relative to ERA5  
322 (Fig. 1j,p).

323

324 Figure 1 shows that the QBOs are too narrow. We calculate the latitudinal extents of the  
325 QBOs at 10 hPa using the “half-maximum” method of Richter et al. (2020) and Bushell  
326 et al. (2020); see the model titles in Fig. 1. Regression between these extents and Asia  
327  $P_{\varphi}$  shows little correlation (Fig. S6). Regardless, Hansen et al. (2013) have already  
328 shown that narrow QBOs coincide with a reduced HTE.

329

## 330 **5 Conclusions**

331 The HTE is analyzed in the CMIP6 historical simulations studied by Richter et al. 2020.  
332 The CMIP6 models consistently underestimate the amplitude of the HTE during  
333 December and January relative to ERA5. This conclusion is robust to three different  
334 QBO indices.

335

336 The underestimation of the HTE coincides with underestimation of the 10 hPa QBO  
337 amplitudes. The desired impact that the models are not representing is the intrusion of  
338 high PV anomalies over Asia. This signal is highly anticorrelated with polar stratospheric  
339 warming taking place during  $\text{QBO}_{E50}$ . The transient simulations in which the QBO is

340 imposed in a live running atmosphere devoid of a QBO, and CPS, which includes no  
341 polar stratospheric variability, both suggest that the QBO promotes the intrusion of high  
342 PV air over Asia *by itself*. Further, the presence of this signal in the CMIP6 models that  
343 simulate HTE, the 1500-year SC-WACCM4 simulation set, and ERA5 suggest this is an  
344 important feature for the teleconnection in nature.

345

346 Why does the PV intrusion occur over Asia? The QBO has a stronger amplitude over  
347 that sector (Fig. S5), but other factors may play a role too. For instance, orographic  
348 gravity wave drag over the Tibetan Plateau has a nonnegligible influence on the  
349 stratospheric mean flow (Xu et al. 2017). This will have to be investigated in future work.

350

### 351 **Acknowledgments, Samples, and Data**

352 High performance computing support is generously provided by the National Center for  
353 Atmospheric Research, sponsored by the National Science Foundation (NSF).

354 doi:10.5065/D6RX99HX. CMIP6 data is archived very nicely and provided by the Earth  
355 System Grid Federation (<https://esgf-node.llnl.gov/search/cmip6/>). Thank you to various

356 modeling agencies who have run the simulations, processed the data, and made it

357 publicly available. ERA5 reanalysis may be accessed with Copernicus

358 ([https://cds.climate.copernicus.eu/cdsapp#!/dataset/10.24381/cds.bd0915c6?](https://cds.climate.copernicus.eu/cdsapp#!/dataset/10.24381/cds.bd0915c6?tab=overview)

359 [tab=overview](https://cds.climate.copernicus.eu/cdsapp#!/dataset/10.24381/cds.bd0915c6?tab=overview)). doi:10.24381/cds.bd0915c6. This study is supported by the NSF,

360 Division of Graduate Education, DGE-1839285, and the Department of Energy, Office of

361 Biological Environment Research, DE-SC0019407. Reviewers, we will add our CPS,

362 AMIP, PAMIP, and transient simulation data to Zenodo once we go through the review

363 process. You can only submit data there once as submitting your data coincides with  
364 receiving a unique doi, which is meant to go in the acknowledgements.

365

366

367

368 **References**

369

370 Andrews, M. B., Knight, J. R., Scaife, A. A., Lu, Y., Wu, T., Gray, L. J., & Schenzinger,  
371 V. (2019). Observed and simulated teleconnections between the stratospheric quasi-  
372 biennial oscillation and Northern Hemisphere winter atmospheric circulation. *Journal of*  
373 *Geophysical Research: Atmospheres*, 124(3), 1219-1232.

374

375 Bushell, A. C., Anstey, J. A., Butchart, N., Kawatani, Y., Osprey, S. M., Richter, J. H., ...  
376 & Yukimoto, S. (2020). Evaluation of the Quasi-Biennial Oscillation in global climate  
377 models for the SPARC QBO-initiative. *Quarterly Journal of the Royal Meteorological*  
378 *Society*.

379

380 Collimore, C. C., Martin, D. W., Hitchman, M. H., Huesmann, A., & Waliser, D. E.  
381 (2003). On the relationship between the QBO and tropical deep convection. *Journal of*  
382 *climate*, 16(15), 2552-2568.

383

384 Elsbury, D., Peings, Y., & Magnusdottir, G. Variation in the Holton-Tan effect by  
385 longitude. *Quarterly Journal of the Royal Meteorological Society*.

386

387 Garfinkel, C. I., & Hartmann, D. L. (2011). The influence of the quasi-biennial oscillation  
388 on the troposphere in winter in a hierarchy of models. Part I: Simplified dry  
389 GCMs. *Journal of the Atmospheric Sciences*, 68(6), 1273-1289.

390

391 Garfinkel, C. I., Shaw, T. A., Hartmann, D. L., & Waugh, D. W. (2012). Does the Holton–  
392 Tan mechanism explain how the quasi-biennial oscillation modulates the Arctic polar  
393 vortex?. *Journal of the Atmospheric Sciences*, *69*(5), 1713-1733.

394

395 Gray, L. J., Anstey, J. A., Kawatani, Y., Lu, H., Osprey, S., & Schenzinger, V. (2018).  
396 Surface impacts of the quasi biennial oscillation. *Atmospheric Chemistry and Physics*,  
397 *18*(11), 8227-8247.

398

399 Hamilton, K., Hertzog, A., Vial, F., & Stenchikov, G. (2004). Longitudinal variation of the  
400 stratospheric quasi-biennial oscillation. *Journal of the atmospheric sciences*, *61*(4), 383-  
401 402.

402

403 Hansen, F., Matthes, K., & Gray, L. J. (2013). Sensitivity of stratospheric dynamics and  
404 chemistry to QBO nudging width in the chemistry–climate model WACCM. *Journal of*  
405 *Geophysical Research: Atmospheres*, *118*(18), 10-464.

406

407 Hersbach, H., Bell, B., Berrisford, P., Hirahara, S., Horányi, A., Muñoz–Sabater, J., ... &  
408 Thépaut, J. N. (2020). The ERA5 global reanalysis. *Quarterly Journal of the Royal*  
409 *Meteorological Society*, *146*(730), 1999-2049.

410

411 Hitchman, M. H., & Huesmann, A. S. (2009). Seasonal influence of the quasi-biennial  
412 oscillation on stratospheric jets and Rossby wave breaking. *Journal of the atmospheric*  
413 *sciences*, 66(4), 935-946.

414

415 Hitchman, M. H., Yoden, S., Haynes, P. H., Kumar, V., & Tegtmeier, S. (2021). An  
416 Observational History of the Direct Influence of the Stratospheric Quasi-biennial  
417 Oscillation on the Tropical and Subtropical Upper Troposphere and Lower Stratosphere.  
418 *Journal of the Meteorological Society of Japan. Ser. II.*

419

420 Huang, B., Hu, Z. Z., Kinter, J. L., Wu, Z., & Kumar, A. (2012). Connection of  
421 stratospheric QBO with global atmospheric general circulation and tropical SST. Part I:  
422 Methodology and composite life cycle. *Climate dynamics*, 38(1-2), 1-23.

423

424 Holton, J. R., & Tan, H. C. (1980). The influence of the equatorial quasi-biennial  
425 oscillation on the global circulation at 50 mb. *Journal of Atmospheric Sciences*, 37(10),  
426 2200-2208.

427

428 Lu, H., Bracegirdle, T. J., Phillips, T., Bushell, A., & Gray, L. (2014). Mechanisms for the  
429 Holton–Tan relationship and its decadal variation. *Journal of Geophysical Research:*  
430 *Atmospheres*, 119(6), 2811-2830.

431

432 Lu, H., Hitchman, M. H., Gray, L. J., Anstey, J. A., & Osprey, S. M. (2020). On the role  
433 of Rossby wave breaking in the quasi–biennial modulation of the stratospheric polar

434 vortex during boreal winter. *Quarterly Journal of the Royal Meteorological*  
435 *Society*, 146(729), 1939-1959.

436

437 Pahlavan, H. A., Fu, Q., Wallace, J. M., & Kiladis, G. N. (2021). Revisiting the quasi-  
438 biennial oscillation as seen in ERA5. Part I: Description and momentum budget. *Journal*  
439 *of the Atmospheric Sciences*, 78(3), 673-691.

440

441 Plumb, R. A., & Bell, R. C. (1982). A model of the quasi-biennial oscillation on an  
442 equatorial beta-plane. *Quarterly Journal of the Royal Meteorological Society*, 108(456),  
443 335-352.

444

445 Rao, J., Garfinkel, C. I., & White, I. P. (2020). Impact of the Quasi-Biennial Oscillation  
446 on the Northern Winter Stratospheric Polar Vortex in CMIP5/6 Models. *Journal of*  
447 *Climate*, 33(11), 4787-4813.

448

449 Rao, J., Garfinkel, C. I., & White, I. P. (2020). How does the Quasi-Biennial Oscillation  
450 affect the boreal winter tropospheric circulation in CMIP5/6 models?. *Journal of Climate*,  
451 33(20), 8975-8996.

452

453 Richter, J. H., Anstey, J. A., Butchart, N., Kawatani, Y., Meehl, G. A., Osprey, S., &  
454 Simpson, I. R. (2020). Progress in simulating the quasi-biennial oscillation in CMIP  
455 models. *Journal of Geophysical Research: Atmospheres*, 125(8), e2019JD032362.

456

457 Smith, K. L., Neely, R. R., Marsh, D. R., & Polvani, L. M. (2014). The specified  
458 chemistry whole atmosphere community climate model (SC–WACCM). *Journal of*  
459 *Advances in Modeling Earth Systems*, 6(3), 883-901.

460

461 Son, S. W., Lim, Y., Yoo, C., Hendon, H. H., & Kim, J. (2017). Stratospheric control of  
462 the Madden–Julian oscillation. *Journal of Climate*, 30(6), 1909-1922.

463

464 Tegtmeier, S., Anstey, J., Davis, S., Ivanciu, I., Jia, Y., McPhee, D., & Pilch Kedzierski,  
465 R. (2020). Zonal asymmetry of the QBO temperature signal in the tropical tropopause  
466 region. *Geophysical Research Letters*, 47(24), e2020GL089533.

467

468 Wang, C. C., & Magnusdottir, G. (2005). ITCZ breakdown in three-dimensional  
469 flows. *Journal of the atmospheric sciences*, 62(5), 1497-1512.

470

471 Wang, J., Kim, H. M., Chang, E. K., & Son, S. W. (2018). Modulation of the MJO and  
472 North Pacific storm track relationship by the QBO. *Journal of Geophysical Research:*  
473 *Atmospheres*, 123(8), 3976-3992.

474

475 Yamashita, Y., Naoe, H., Inoue, M., & Takahashi, M. (2018). Response of the Southern  
476 Hemisphere atmosphere to the stratospheric equatorial quasi-biennial oscillation (QBO)  
477 from winter to early summer. *Journal of the Meteorological Society of Japan. Ser. II.*

478

479

480

481 **Figure 1.** Figure 1: DJ zonal mean zonal wind anomalies. Thin contours show  
 482 anomalies between +/- 8.5 m/s with intervals of +/- 1m/s. Thick contours correspond to  
 483 +10, 15, 20 ... m/s. Gray shading denotes statistical significance, p-values < 0.05 via a  
 484 student's t-test, when comparing QBO<sub>E50</sub> anomalies to all other anomalies. To the right  
 485 of model titles is the number of DJ periods averaged together to make each composite  
 486 and the 10 hPa latitudinal width of the QBO. Widths are calculated by applying the "half-  
 487 maximum" method of Richter et al. (2020) and Bushell et al. (2020) to the anomalous 10  
 488 hPa response from each plot. Warm (cool) temperature anomalies are shown on Fig. 1q  
 489 with +/- 1 K contours.

490

491 **Figure 2:** ERA5 DJ 850 Kelvin PV anomalies. Anomalies are deviations from the  
 492 seasonal cycle for QBO<sub>E50</sub> indices. Hatching denotes statistical significance, p-values <  
 493 0.05 via a student' t-test, when comparing QBO<sub>E50</sub> anomalies to all other anomalies. The  
 494 contour interval in line and shading for all panels is +/- 10 PVU. Fifteen DJ seasons are  
 495 used to make the composite (a). Panel (b) shows the standard deviation of the field with  
 496 contour intervals 10, 20, 30... PVU.

497

498 **Figure 3:** Anomalies after imposing a QBO<sub>E50</sub> profile in the transient runs. (a-c): Zonal  
 499 mean meridional PV gradient for successive 30-day periods after branching: dashed-  
 500 negative (solid-positive) contours begin at negative (positive)  $1 \times 10^{-7} \text{ K} \cdot \text{m} \cdot \text{kg}^{-1} \cdot \text{s}^{-1}$  and  
 501 decrease (increase) by negative (positive)  $5 \times 10^{-7} \text{ K} \cdot \text{m} \cdot \text{kg}^{-1} \cdot \text{s}^{-1}$  intervals. The responses  
 502 at each isentrope are multiplied by  $(/350)^{-9/2}$  to account for logarithmic change in PV with

503 height. (d-f): Latitude-time Hövmollers of 850 Kelvin PV (+/- 10 PVU) averaged over  
504 0°E-120°E (d), 120°E-240°E (e), and (f) 240°E-360°E. Gray shading denotes statistical  
505 significance in (a-f), p-values < 0.05 via a student's t-test, when comparing QBO<sub>E50</sub> and  
506 control responses. (g-h) Maps of 850 K PV (+/- 10 PVU) anomalies with hatching  
507 denoting statistical significance.

508

509 **Figure 4:** DJ 850 K PV anomalies for the 18 datasets. Contour intervals are +/- 10 m/s.  
510 Hatching denotes statistical significance, p-values < 0.05 via a student's t-test, when  
511 comparing QBO<sub>E50</sub> anomalies to all other anomalies. Black and blue rectangles denote  
512 where the anomalous  $\rho$  is highly correlated with polar cap warming (Table S1).

513

514 **Figure 5:** Left: The anomalous meridional PV gradient ( $\rho$ ) over Asia is compared to the  
515 anomalous 10 hPa polar cap (60°N+) temperature.  $\rho$  is not divided by the radius of  
516 Earth when calculating it. Right: The anomalous 10 hPa QBO, longitudinally averaged  
517 and cosine weighted latitudinally averaged zonal winds between 5°S-5°N, of Figure 1  
518 are compared to  $\rho$  over Asia.